RSC Advances

PAPER

View Article Online
View Journal | View Issue

Cite this: *RSC Adv.*, 2025, **15**, 22565

Effects of iron oxide-modified hierarchically porous 4A zeolites on flame retardancy of ammonium polyphosphate-treated wood composites

Shaodi Zhang, [ab] Mingzhi Wang,*[b] Yuxiang Huang, [a] Yahui Zhang[a] and Wenji Yu *[a]

The combination of inorganic porous nanomaterials with metal oxides has shown great prospects as flame retardants or flame-retardant synergists in wood composites. In this work, iron oxide-modified hierarchically porous 4A (FeH4A) zeolites were prepared and applied as synergists of ammonium polyphosphate (APP) for flame retardant treatment of wood composites. The effects of FeH4A zeolites with various degrees of modification (0.5FeH4A, 1FeH4A, 5FeH4A, and 10FeH4A) on flame retardancy of wood composites were investigated. With proper modification, the 0.5FeH4A zeolite favored the decomposition process of APP at low temperatures, leading to better flame retardancy. The peak heat release rate (HRR) and total heat release (THR) of W-APP-0.5 FeH4A were decreased by 15.8% and 16.7%, respectively, compared with those of W-APP-H4A. However, severe modification results in damage of the zeolite framework. This change along with the excess iron oxide weaken the thermal stability of the char residue, which negatively affects flame retardancy. Further investigation of the pyrolysis products and morphologies of the char residue indicates that the FeH4A zeolites play a role in both gaseous and condensed phase flame-retardant mechanisms. This study provides information for the development of novel flame retardants and effective synergists for wood composites.

Received 4th May 2025
Accepted 24th June 2025

DOI: 10.1039/d5ra03148f

rsc.li/rsc-advances

1. Introduction

Considering sustainability, energy/resource conservation, and strength/weight ratio, wood composites have become promising materials for construction and building applications.[1,2] However, the inherent flammability of wood composites poses significant risks to human life and properties. Common strategies for addressing this issue include incorporating flame retardants during manufacturing or applying flame-retardant coatings on composite surfaces. Ammonium polyphosphate (APP) is a common halogen-free flame retardant for wood-based materials.[3,4] Nevertheless, a large amount of APP must be added to the substrate to obtain satisfactory flame retardancy. A high flame-retardant content negatively affects the mechanical properties, which restricts the application of wood composites.[5] Therefore, it is essential to develop high-efficiency flame retardant systems.[6–8]

Recently, inorganic nanomaterials such as montmorillonite (MMT),[9] layered double hydroxides (LDHs),[10] metal–organic frameworks (MOFs)[11] and zeolites[12,13] have been combined with APP to improve their flame-retardant efficiency. Zeolites are crystalline aluminum silicates with a three-dimensional framework and porous structure.[14] Owing to their large surface area and high thermal stability, zeolites have gained attention for flame-retardant applications in polymeric and wood-based materials.[12,15,16] Zeolites could effectively promote the formation of thermally stable char layers, thus reducing the pyrolysis intensity and production of flammable volatiles along with APP.[13] It has been proved that the pore structure has a significant effect on the flame-retarding performance of zeolites. In our previous work, hierarchically porous 4A (H4A) zeolites were synthesized and used as additives to APP. We found that H4A zeolites can inhibit fire growth and restrict smoke and CO production more significantly than microporous 4A zeolites owing to their ability of accelerating APP decomposition.[16] Moreover, larger mesopore diameter of H4A zeolites favors better smoke suppression performance due to the improved mass transfer,[17] suggesting great prospects for the flame-retardant treatment of wood composites.

Despite the above-mentioned nanomaterials, traditional metal salts and oxides are also selected as additives of flame retardants to improve flame-retardant efficiency owing to their catalytic effects and low cost.[18,19] They show good flame retardancy and smoke suppression, either alone or in combination with other phosphorus-based flame retardants. In Davies' study, transition metal ions promoted the decomposition of APP at lower temperatures, thereby enhancing the flame

[a]*Research Institute of Wood Industry, Chinese Academy of Forestry, Beijing 100091, China. E-mail: chinayuwj@126.com*

[b]*MOE Key Laboratory of Wooden Material Science and Application, Beijing Forestry University, Beijing, 100083, China. E-mail: wmingzhi@bjfu.edu.cn*

retardancy of cellulose.[20] Chen *et al.* found that iron oxide green,[21] iron oxide brown,[22] and ferrite yellow[23] can reduce the heat release rate and smoke production of intumescent flame-retardant (APP and pentaerythritol)-treated epoxy composites. Notably, transition metal ions or oxides exhibited a synergistic effect with other inorganic nanomaterials to improve flame retardancy. For instance, Fe_2O_3 modified MMT exhibited remarkably improved flame-retarding and smoke-suppressing properties compared to pure MMT.[24] Yang *et al.* modified ZSM-5 zeolite with copper using the impregnation method (500Cu-Z), and the prepared 500Cu-Z was applied as an additive to APP-treated pulp.[25] It was discovered that 500Cu-Z had a synergistic flame-retardant effect with APP. The Cu^{2+} in the ZSM-5 zeolites catalyzed CO to CO_2 and effectively reduced smoke toxicity.

These works suggested that the combination of zeolites and metal ions or oxides shows great potential for improving the flame retardancy of wood composites. Our previous study have demonstrated the superior effects of hierarchically porous zeolites on inhibiting fire growth and restricting smoke and CO production.[13,16,17] The hierarchical porosity of zeolites could facilitate the incorporation of metal oxides within nanomaterials,[26,27] which will enhance the combining effects. However, the zeolite framework could be destroyed when the modification degree is too heavy. Excessive inorganics may also make the char layer fragile, thus negatively affects the flame retardancy.[28] How will metal ions or oxides affect the flame-retardant performance of nanomaterials with hierarchical porosity in wood composites remains an unsolved question.

In this study, iron oxide-modified H4A zeolites (FeH4A) were prepared and applied as additives in APP-treated wood composites. The flame-retardant performance of as prepared wood composites was evaluated using cone calorimetry test (CCT). The thermal degradation behaviors of the flame-retardant system and treated wood composites were analyzed using thermal gravimetric (TG) analysis. Furthermore, the gaseous products generated during pyrolysis were analyzed using thermogravimetry-Fourier transform infrared (TG-FTIR) spectroscopy to elucidate the flame-retardant mechanisms.

2. Experimental

2.1 Materials

Poplar (Polulus tomentosa Carr.) wood flour (mesh size of 10–60) was obtained from Xingda Wood Flour Company, Gaocheng, China. The wood flour was dried in an oven at 103 °C for 8 h to obtain a moisture content of 3% prior to fabricating the wood composites. Phenol formaldehyde (PF, solid content of 45%, viscosity of 100–150 mPa s, and pH value of 11–12) resin was provided by Hengtai Chemical Industry Company, Jining, China. APP (n > 1000) was supplied by Ji'nan Taixing Fine Chemical (Ji'nan, China) as a flame retardant. Sodium hydroxide (NaOH, AR), sodium aluminate ($NaAlO_2$, AR), and sodium metasilicate nonahydrate ($NaSiO_2 \cdot 9H_2O$, AR) were purchased from Beijing Chemical Works (Beijing, China). Dimethyloctadecyl [3-(trimethoxysilyl) propyl] ammoniochloride (DTPAC, 60 wt% in methanol) and $Fe(NO_3)_3 \cdot 9H_2O$ (AR, Beijing) were purchased from J&K Chemical (Shanghai, China) and Beijing Innochem Science & Technology (Beijing, China), respectively. All chemicals were used as received without further purification.

2.2 Preparation of FeH4A

The H4A zeolite was synthesized using the soft-template method, as previously described.[29] For the iron oxide modification of the H4A zeolite, a wetness impregnation method was used. Aqueous solution of Fe^{3+} with different concentration was prepared first by dissolving different amount (Fe^{3+} weight = 0.5/1/5/10 wt% of H4A zeolite) of $Fe(NO_3)_3 \cdot 9H_2O$ into 100 grams of deionized water. Next, 10 g of H4A zeolite was added to the solution with a magnetic stirring at 60 °C for 3 h. The solid was collected by filtration and washed with deionized water until the pH of the rinse liquid reached 7. Then the modified zeolite was dried in an oven at 110 °C for 3 h, and subsequently at 80 °C for 24 h. Finally, the obtained product was calcined at 500 °C in air for 4 h. The resulting samples are denoted as nFeH4A (where n represents the Fe^{3+} weight percent, n = 0.5/1/5/10).

2.3 Characterization

X-ray diffraction (XRD) patterns of the samples in the range of 2θ = 5–50° of the samples were obtained using a Bruker D8 Advanced X-ray diffractometer (Billerica, USA) equipped with a Cu Kα radiation source at 40 kV and 40 mA with an angular step size of 0.02°. Field emission scanning electron microscopy (FE-SEM) images were recorded using a Hitachi S-4800 Scanning Electron Microscope (Tokyo, Japan). An automated physisorption analyzer (Autosorb iQ Station 2, Quantachrome Instruments, Boynton Beach, USA) was used to measure the N_2 adsorption/desorption isotherms of the samples at −196 °C. The pore size distributions were calculated using the Barrett–Joyner–Halenda (BJH) formula based on the adsorption branch. X-ray photoelectron spectroscopy (XPS) analyses were conducted on a Thermo ESCALAB 250Xi 165 (Thermo Scientific, USA) instrument using Kα excitation radiation ($h\gamma$ = 1486.6 eV).

2.4 Fabrication of wood composites

Flame-retardant wood composites were prepared according to the procedure described in our previous study.[13] The PF resin and flame retardants were 10 and 20 wt% of wood flour, respectively. The mass ratio of APP to zeolites was APP : FeH4A = 19 : 1. All of the samples were prepared by carefully controlling the weight of raw materials, including wood flour, resin, and flame retardants, to ensure small variability.

2.5 Thermal stability, pyrolytic products, and combustion behavior analysis

A thermogravimetric analyzer (TGA Q5000, TA instruments, New Castle, USA) was used to investigate the thermal degradation behavior of the samples. Approximately 20 mg of flame retardant with a particle size of less than 150 μm was heated from 30 °C to 800 °C at a heating rate of 10 °C min^{-1} under N_2. Thermal analysis of the wood composites was conducted in an air atmosphere. Thermogravimetry-Fourier transform infrared

(TG-FTIR) spectroscopy was conducted by coupling a Spectrum GX spectrometer (PerkinElmer, Fremont, USA) to the TG analyzer to investigate the gaseous products when the samples were tested.

A cone calorimetry test was performed to evaluate the combustion behavior using an cone calorimeter (FTT00007, FTT, West Sussex, England) according to the ISO 5660-2 standard. Wood composite samples with dimensions of 100 × 100 × 10 mm were wrapped with pre-cut aluminum foil and exposed to an external heat flux of 50 kW m^{-2}. Three replicates were tested for each group.

3. Results and discussion

3.1 Characterization of iron oxide modified H4A zeolites

The SEM images of the zeolites are shown in Fig. 1. Fig. 1a and b revealed that the H4A zeolite exhibited a global-cubic morphology with rugged surfaces, indicating the presence of mesopores.[30] The practical size of the H4A zeolites is 2–5 μm. With the modification process, it was clear that amorphous iron oxides were deposited on the surface of 0.5FeH4A (circles in Fig. 1d). For 10FeH4A (Fig. 1e and f), many fragments were exfoliated, probably because of dealumination in an acidic environment.[31] In contrast to H4A and 0.5FeH4A, the apertures on the surfaces of the 10FeH4A particles disappeared, indicating the presence of abundant iron oxide on the surfaces of the zeolites. Some macropores can be observed in the inset image of Fig. 1f owing to the break of the framework.

The synthesis of FeH4A zeolites was further confirmed by N_2 adsorption–desorption isotherms and XRD results (Fig. 2a and c). The pore structures of the samples are listed in Fig. 2b and Table 1. H4A zeolite exhibited an average mesopore diameter of 8.92 nm (Fig. 2b). After modification, the average mesopore diameter of 0.5FeH4A was similar to that of the H4A zeolite

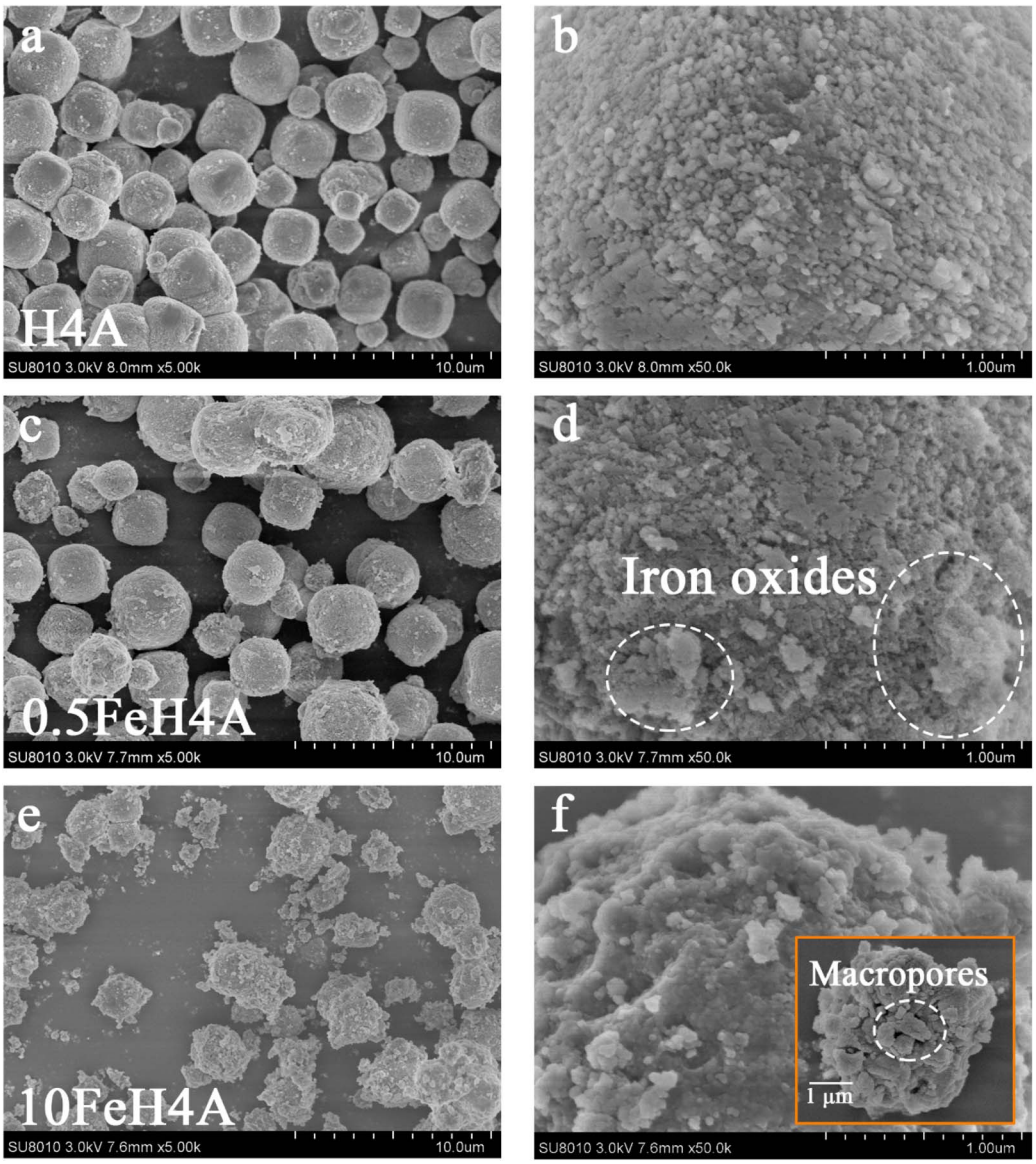

Fig. 1 SEM images of (a and b) H4A zeolite and (c–f) iron oxide modified H4A zeolites. (c and d) 0.5FeH4A, (e and f) 10Fe H4A.

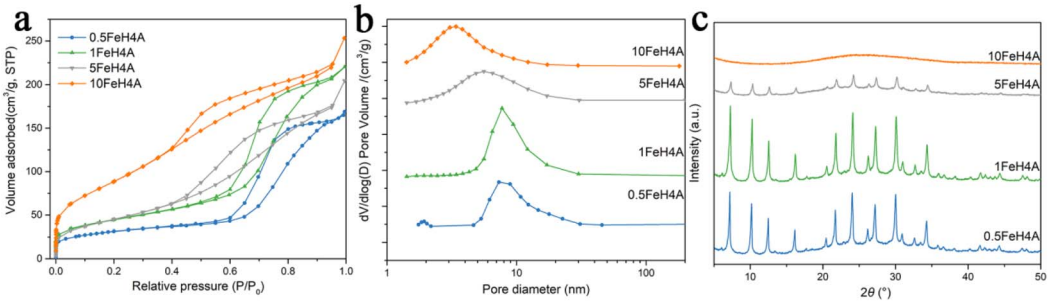

Fig. 2 (a) N_2 adsorption–desorption isotherms, (b) BJH pore diameter distributions, and (c) XRD patterns of H4A zeolites.

Table 1 Pore structure data of H4A zeolites

	Fe^{3+} amount in solution (wt% of H4A zeolites)	Fe^{3+} content in zeolite (wt%)	BET surface areas ($cm^2\ g^{-1}$)	Pore diameters (nm)
H4A	—	—	120.16	8.92
0.5FeH4A	0.5	2.49	101.78	9.34
1FeH4A	1	2.99	158.20	7.73
5FeH4A	5	3.93	168.92	5.59
10FeH4A	10	6.93	338.19	3.40

(9.34 nm). With an increase in Fe^{3+}, the pore diameter decreased gradually (Table 1). The XRD results in Fig. 2c show the characteristic peaks of the crystalline LTA zeolites, which is in accordance with previously reported studies.[30] However, no strong characteristic peaks were detected for 10FeH4A, suggesting that the crystalline structure was probably destroyed when the H4A zeolite was modified in a high-concentration $Fe(NO_3)_3$ solution.

The Fe 2p XPS spectra of FeH4A were recorded, and the results are illustrated in Fig. 3a and b. Two characteristic peaks of Fe $2p_{1/2}$ and Fe $2p_{3/2}$ can be observed at 725.3 and 711.3 eV, respectively. Satellite peaks situated at approximately 719 eV can be found, which is similar to the results in previous reports for Fe_2O_3,[32,33] indicating the formation of amorphous Fe_2O_3 within the samples.

Based on these results, the structure and morphology of zeolites can be well characterized. During the modification process, iron oxide (Fe_2O_3) particles were simultaneously deposited on the surface and introduced into the inner part of the H4A zeolite at the same time, resulting in a smaller mesopore diameter. The crystalline structure of H4A zeolite remained stable when the concentration of the $Fe(NO_3)_3$ solution was low. However, higher concentrations of $Fe(NO_3)_3$ could lead to the partial destruction of the crystalline framework of the H4A zeolites. Abundant iron oxide deposit in the channel and on the surface of H4A zeolites, forming large amounts of micro- and mesopores and leading to increased surface area (Table 1).[34]

3.2 Combustion behavior of wood composites

CCT was conducted to assess the flame retardancy of the wood composites. The results are presented in Fig. 4 and Table 2. Almost all CV values of the results are less than 10%, indicating

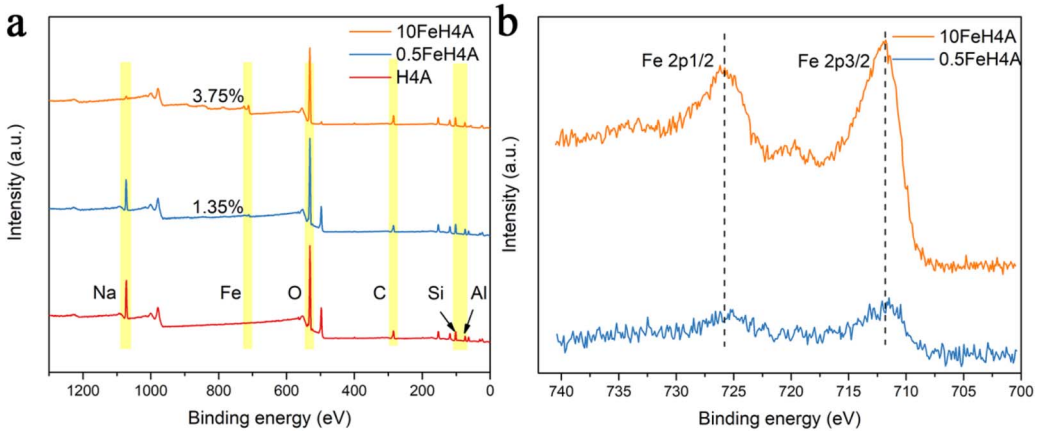

Fig. 3 (a) XPS survey scans and (b) high resolution Fe 2p XPS spectra of samples.

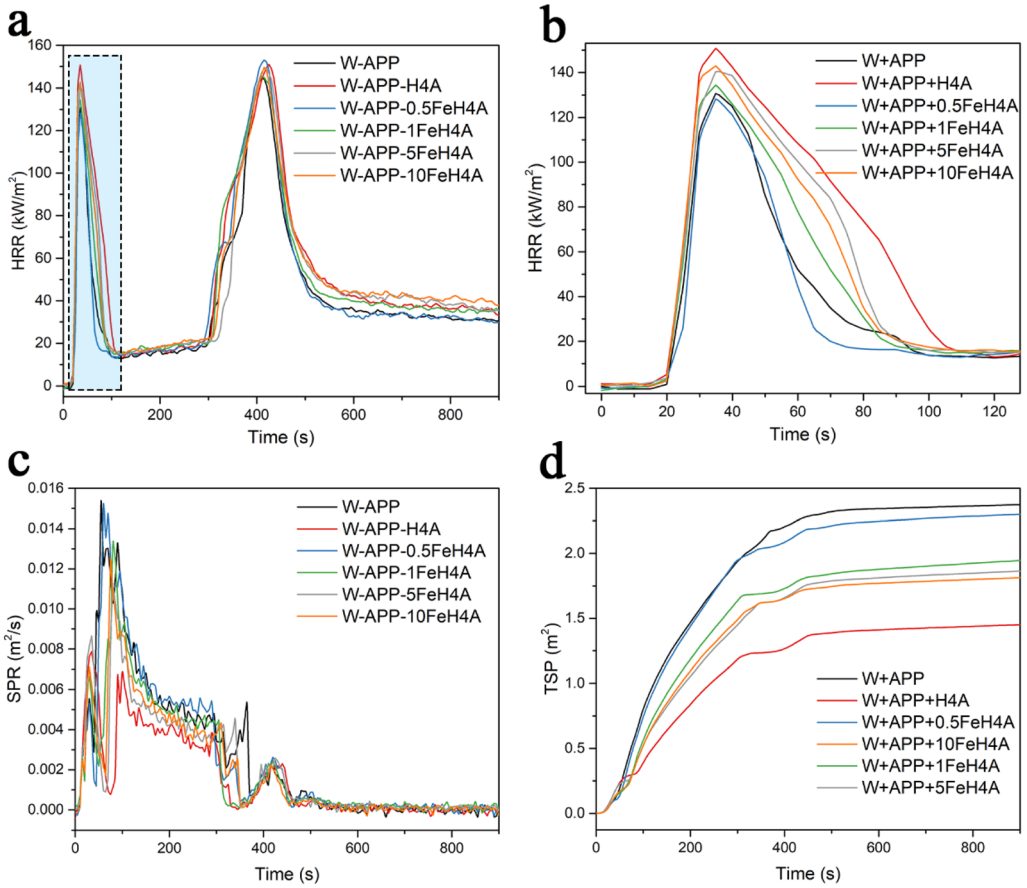

Fig. 4 HRR (a and b), smoke production rate (SPR, c) and total smoke production (TSP, d) curves of different samples.

high reliability. Typical two-peak HRR curves can be observed in Fig. 4a, which are in accordance with previous studies.[35] The combustion process is divided into four stages. The first heat release peak ($PHRR_1$) was attributed to the violent burning (*i.e.*, flame combustion) of the surface material in the first stage (t < 100 s). A carbonaceous char layer was produced after the combustion of the surface. This char layer played an essential role in preventing intense combustion of the substrate. In the second stage (100 s < t < 300 s), flame combustion was suspended and glowing combustion occurred. The smoke was released quickly during the first stage and gradually reduced during the second stage (Fig. 4c). The surface char layer broke down in the third stage (300 s < t < 500 s), leading to a second heat release peak ($PHRR_2$). At the last stage (t > 500 s), flame combustion ceased, and glowing combustion occurred again.

APP-H4A treated wood composites showed slightly higher $PHRR_1$ (Fig. 4b) and THR values (Table 2) than the APP-treated group, but produced much less smoke and CO due to the adsorption effect of H4A zeolites.[17] With the addition of 0.5FeH4A, the $PHRR_1$ and THR of W-APP-H4A decreased from 152.51 ± 8.43 kW m^{-2} and 48.12 ± 1.70 MJ m^{-2} to 128.84 ± 6.27 kW m^{-2} and 40.08 ± 2.31 MJ m^{-2}, respectively, suggesting that the earlier decomposition of APP can promote the char formation and restrict the flame combustion. Although the reduction is minor, the THR of W-APP-H4A is less than W-APP. In previous studies, although H4A zeolites could play significant role in

Table 2 CCT data of different samples

Group	$PHRR_1$ (kW m^{-2})	T1[a] (s)	FGI (kW m^{-2} s^{-1})	THR (MJ m^{-2})	TSP (m^2)	COY ($\times 10^{-4}$ kg kg^{-1})
W-APP	131.85 ± 5.35[b]	33.33	3.96	38.65 ± 4.43[c]	2.79 ± 0.52	635 ± 51
W-APP-H4A	152.51 ± 8.43	33.33	4.72	48.12 ± 1.70	1.44 ± 0.01	526 ± 22
W-APP-0.5FeH4A	128.84 ± 6.27	35.00	3.68	40.08 ± 2.31	2.13 ± 0.09	660 ± 53
W-APP-1FeH4A	134.77 ± 5.02	35.00	3.85	43.50 ± 2.06	1.93 ± 0.19	558 ± 30
W-APP-5FeH4A	144.28 ± 2.47	35.00	4.12	44.72 ± 1.04	1.85 ± 0.05	574 ± 49
W-APP-10FeH4A	143.33 ± 3.65	33.33	4.30	45.54 ± 3.67	1.80 ± 0.33[c]	561 ± 48

[a] T1, time to $PHRR_1$. [b] Standard deviation (SD). [c] Coefficient of variation (CV, SD/mean value) > 10%.

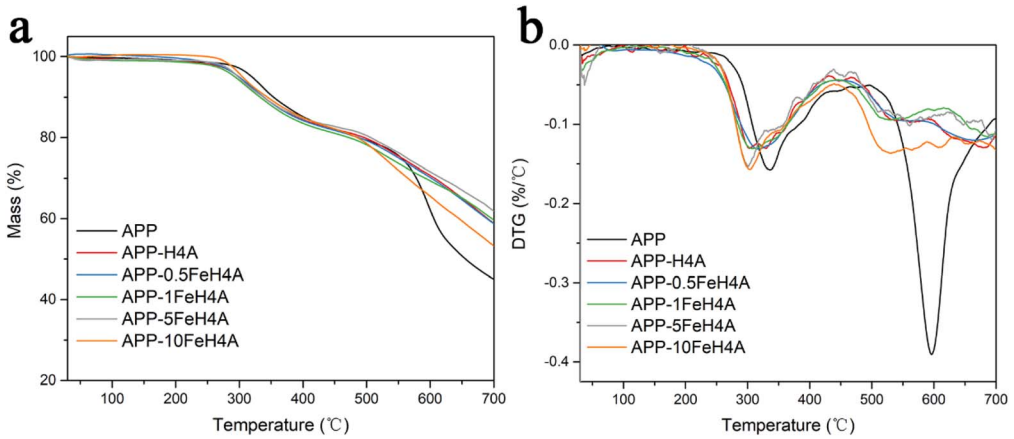

Fig. 5 TG (a) and DTG (b) curves of flame retardants.

restricting smoke emission, it showed no obvious effect on inhibiting THR.[11,15] Hence, APP-modified H4A system exhibited improved flame-retardant efficiency. When the iron oxide content increased, heat release also increased. The $PHRR_1$ and THR of 5FeH4A treated wood composites were 12.0% and 11.6% higher than those of W-APP-H4A. The flame growth index (FGI, PHRR/time to PHRR) is typically used to evaluate the spread rate of a fire. The FGI was reduced from 4.72 kW m^{-2} s^{-1} for W-APP-H4A to 3.68 kW m^{-2} s^{-1} for W-APP-0.5FeH4A, and further increased to 4.30 kW m^{-2} s^{-1} for W-APP-H4A with high iron content. This can be explained by the catalytic degradation of cellulose over iron oxide and the crack of char residue. In addition, a better smoke suppression performance and smaller CO yield (COY) were observed for the 5FeH4A and 10FeH4A treated samples (Fig. 4c, d and Table 2). This is because iron oxide can act as a catalyst to convert CO and other partially oxidized molecules, resulting in less smoke and CO production.[36]

3.3 Thermal behavior of flame retardants

Fig. 5 shows the TG and DTG curves of the different flame retardants. APP decomposition can be divided into two stages (Fig. 5a). The first stage occurs at approximately 200–450 °C is attributed to the formation of ammonia, water, a highly cross-linked polyphosphoric acid, and P_4O_{10}.[20,37] The maximum decomposition rate (R_{max1}) of this stage was 0.157%/°C at 335 °C (T_{max1}). At higher temperatures, the ultraphosphate structure produced from last sage broke down and P_4O_{10} was evaporated, leaving 45.04% of residue at 700 °C. With the addition of H4A zeolites, R_{max1} of APP-H4A was slightly reduced and shifted to a lower temperature (Fig. 5b). This was caused by the acidity of the zeolites, which catalyzed the decomposition of APP.[13] In the second stage, a significantly lower decomposition rate can be detected at lower temperature (approximately 30 °C lower) compared with pure APP (Table 3). This was probably due to the reaction of silicon/aluminum compounds with phosphorus.[38] A more stable intumescent char was produced at 700 °C, leaving 58.87% residue.

Compared with APP-H4A, iron oxide modified H4A zeolites further decreased the T_{max1} to 315 °C, 307 °C, 299 °C, and 304 °C for APP-0.5FeH4A, APP-1FeH4A, APP-5FeH4A, and APP-10FeH4A, respectively. Meanwhile, the R_{max1} increased to 0.152%/°C and 0.156%/°C for APP-5FeH4A and APP-10FeH4A, respectively, indicating that the first decomposition process was accelerated by iron oxide. Same trends can be found in the second stage, at which the R_{max2} increased from 0.095%/°C for APP-0.5FeH4A to 0.136%/°C for APP-10FeH4A. This means that excessive iron oxide could negatively affects the stability of the char residue. The residue of APP-10FeH4A at 700 °C was the least (53.22%) among the APP-zeolite systems owing to the improved thermal decomposition rate.

In summary, the H4A zeolite can catalyze the decomposition of APP at low temperatures and form a stable char at higher temperatures. The iron oxide modification of H4A zeolites

Table 3 TGA results of flame retardants

Group	R_{max1}[a] (% °C^{-1})	T_{max1}[a] (°C)	R_{max2}[a] (% °C^{-1})	T_{max2}[a] (°C)	Residue (%)
APP	0.157	335	0.390	597	45.04
APP-H4A	0.130	329	0.097	561	58.87
APP-0.5FeH4A	0.131	315	0.095	554	58.76
APP-1FeH4A	0.130	307	0.094	526	59.68
APP-5FeH4A	0.152	299	0.101	561	61.87
APP-10FeH4A	0.156	304	0.136	530	53.22

[a] R_{max1} and R_{max2} are the maximum decomposition rates in the first and second stages, respectively. Where T_{max1} and T_{max2} the temperatures at R_{max1} and R_{max2}, respectively.

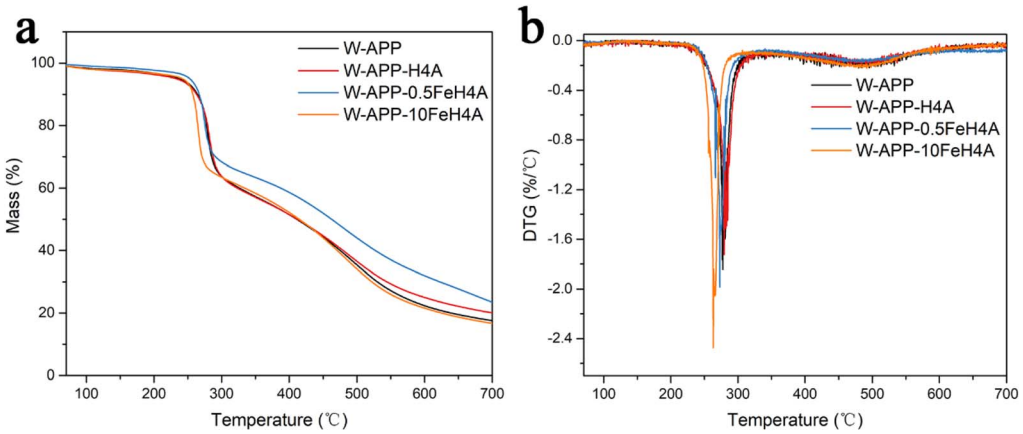

Fig. 6 (a) TG and (b) DTG curves of wood composites in air atmosphere.

favored the first decomposition process of APP, but it decreased the stability of the char residue when the modification degree was too high.

3.4 Thermal stability of wood composites

TG analysis under an oxidative atmosphere was conducted to simulate the thermal decomposition of wood composites in a real fire scenario. After the evaporation of absorbed water, the degradation process can be divided into two stages, namely, the charring stage at 200–300 °C and the calcining stage at higher temperatures (Fig. 6a). At the charring stage, the main components of wood, including hemicellulose and cellulose, are dehydrated, pyrolyzed, and rearranged to produce char residue. At this stage, the post curing and oxidative degradation of PF resin also occurred. Oxidative calcination of the char residue and lignin occurred during the calcining stage. This stage corresponds to further degradation and oxidation of lignin and residual char from the charring stage.

The residue of W-APP at 700 °C increased from 17.57% to 20.05% for W-APP-H4A and 23.49% for W-APP-0.5FeH4A, showing better charring ability. Notably, the addition of iron oxide-modified H4A zeolites increased the first maximum mass loss rate peak (R_{max1}) and shifted this peak to a lower temperature (Fig. 6b and Table 4). This result is supported by the TG results for the flame retardants. Because iron oxide-modified H4A zeolites favor the decomposition of APP to produce phosphorus acid, they can accelerate the dehydration of hemicelluloses and cellulose to form more char at low temperature. Fewer substrates were consumed during this stage, as illustrated in Table 4. When the modification degree was too high, the structure of H4A zeolite was destroyed and the thermal stability of it could be decreased. Also, excess iron oxide could negatively affected the stability of the char residue.[28] The second maximum mass loss rate peak (R_{max2}) increased from 0.17%/°C for W-APP-H4A to 0.22%/°C for W-APP-10FeH4A, resulting in a higher mass loss. Overall, 0.5FeH4A showed the highest residue owing to its good charring effect and the relatively high thermal stability of the char residue. This can explain the CCT results, in which the 0.5FeH4A treated wood composites showed the smallest HRR_1.

3.5 Gaseous products analysis

The investigation of decomposition products can help us understand how iron oxide-modified H4A zeolites affect the decomposition process of wood components. The 3D TG-FTIR spectra of the samples at different temperatures are shown in Fig. 7. It is clear that the pyrolysis products of all samples were similar. Compared to W-APP, W-APP-H4A exhibited much smaller infrared absorption intensity peaks because of the adoption and catalytic properties of H4A zeolites (Fig. 7a and b), as discussed in our previous work.[17] The 0.5FeH4A and 10FeH4A treated wood composites showed no obvious differences from H4A treated sample (Fig. 7c and d).

The Gram–Schmidt (GS) curves, FTIR spectra at different temperatures, and specific products evolved during the thermal decomposition process for different samples are illustrated in Fig. 8. From the GS curves, it can be observed that all the samples have two peaks corresponding to the two stages

Table 4 TGA data of wood composites in air atmosphere

Group	Range	R_{max1} (%/°C)	T_{max1} (°C)	Mass loss (%)	Range (°C)	R_{max2} (%/°C)	T_{max2} (°C)	Mass loss	Residue 700 °C (%)
W-APP	200–320	1.85	277	36.02	320–700	0.22	495	43.18	17.57
W-APP-H4A	200–327	1.72	279	36.82	327–700	0.17	483	39.48	20.05
W-APP-0.5FeH4A	200–336	1.98	272	33.16	336–700	0.19	485	41.08	23.49
W-APP-10FeH4A	200–300	2.48	263	33.24	300–700	0.22	485	46.81	16.67

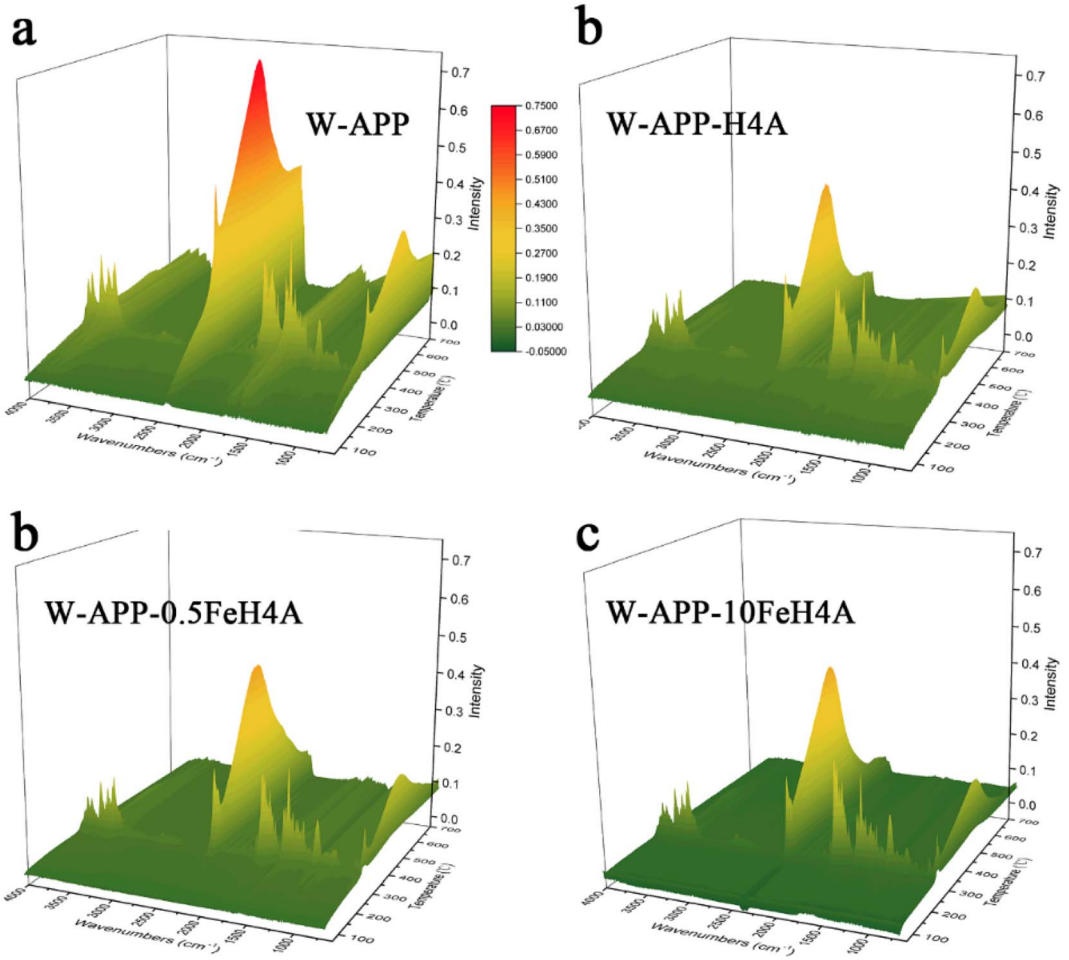

Fig. 7 3D TG-FTIR spectra of (a) W-APP, (b) W-APP-H4A, (c) W-APP-0.5FeH4A, and (d) W-APP-10FeH4A under air atmosphere.

discussed previously. Compared with the APP-treated sample, the first gas release peaks of the H4A and iron oxide-modified H4A zeolites were sharper, and their second gas release peaks were significantly reduced by around 26% (Fig. 8a). As shown in Fig. 8b, the products in the first stage were complicated. Aldehydes/esters/acids (1600–1800 cm^{-1}, C=O), CO_2 (2358 cm^{-1}), hydrocarbons (C–H, 2800–3000 cm^{-1}), and water (3500–3850 cm^{-1}) were detected.[39] In the second stage, CO_2 originated from the oxidation of char residue, which was the main product (Fig. 8c).

For H4A treated samples, the absorption peak intensity of water increased by 12% and shifted to lower temperatures (Fig. 8d) on the same sample weight basis, indicating the catalyzed decomposition of APP or dehydration of polysaccharides.[40,41] The introduction of iron oxide-modified H4A zeolites further reduces the temperature. This could be ascribed to the Lewis acidity of the iron oxides. The characteristic peaks of hydrocarbons were flat for W-APP-0.5FeH4A, and the production of C=O compounds decreased by about 15% compared to W-APP, suggesting the formation of less combustible gases. However, the excessive loading of iron oxide within H4A resulted in a larger C=O peak (Fig. 8e). The increased water production can be explained by the fact that 10FeH4A favors the first decomposition process of APP, which has already been proven in the TG analysis of flame retardants. The increase in C=O compound production may be attributed to the decarboxylation of cellulose over iron oxide,[42] which had a negative effect on the formation of a thick char layer during combustion.

Moreover, the 0.5FeH4A and 10FeH4A treated samples showed lower CO peak intensity in both stages than H4A treated sample (decreased by 18%, Fig. 8f). 10FeH4A with a larger surface area and more active sites on its surface should facilitate the adsorption and catalysis of CO and other uncondensed smoke precursor.[36]

3.6 Char residue analysis

Other than gaseous pyrolytic products, solid char residue was obtained after combustion of wood composites. As a thermal-charring material, wood composites during combustion formed a protective char layer on the surface, which play a key role in affecting flame retardancy.

The morphology of the char residue after CCT is shown in Fig. 8. An intumescent structure was found on the surface of the char residue of W-APP, and deep gaps appear between the

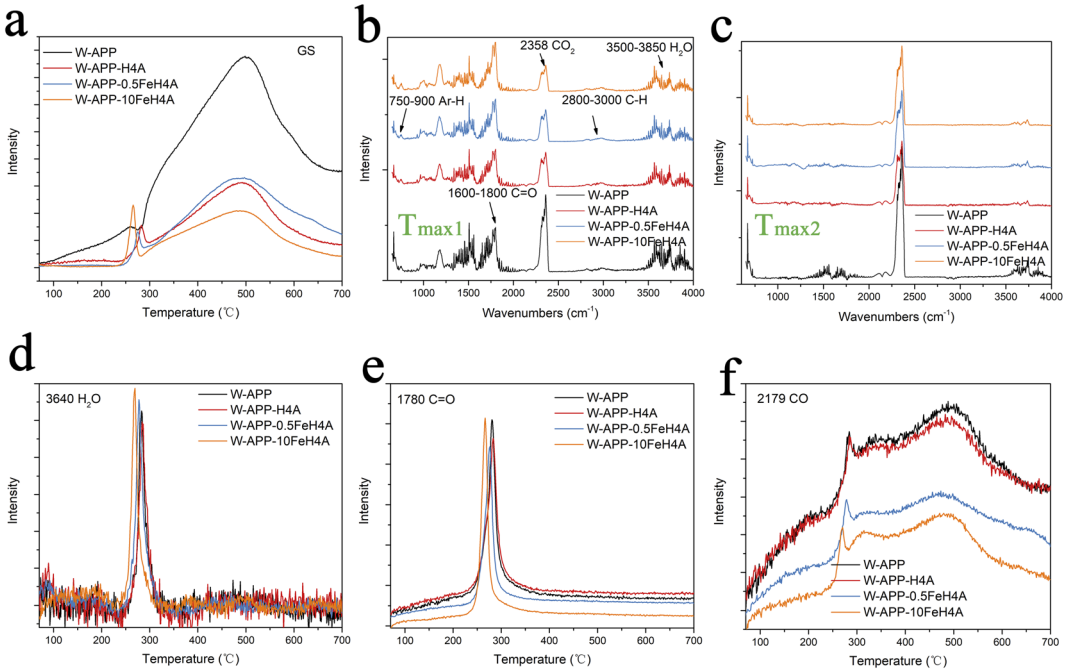

Fig. 8 (a) Gram-Schmidt (GS) curves and FTIR spectra at (b) T_{max1} and (c) T_{max2} of different samples. (d) Water at 3640 cm^{-1}, (e) C=O compounds at 1780 cm^{-1}, and (f) CO at 2179 cm^{-1} evolved during the thermal decomposition process.

intumescent structures (Fig. 9a). W-APP-H4A exhibited small bubbles on the char surface with few cracks (Fig. 9b). A consecutive and intact intumescent structure is observed on the char surface of W-APP-0.5FeH4A (Fig. 9c). The intact surface could effectively restrict the heat transfer and prevent the underlying wood composites from violent pyrolysis, resulting in a lower heat release rate. It is also notable that there are many small cracks and pores on the intumescent structure of W-APP-10FeH4A

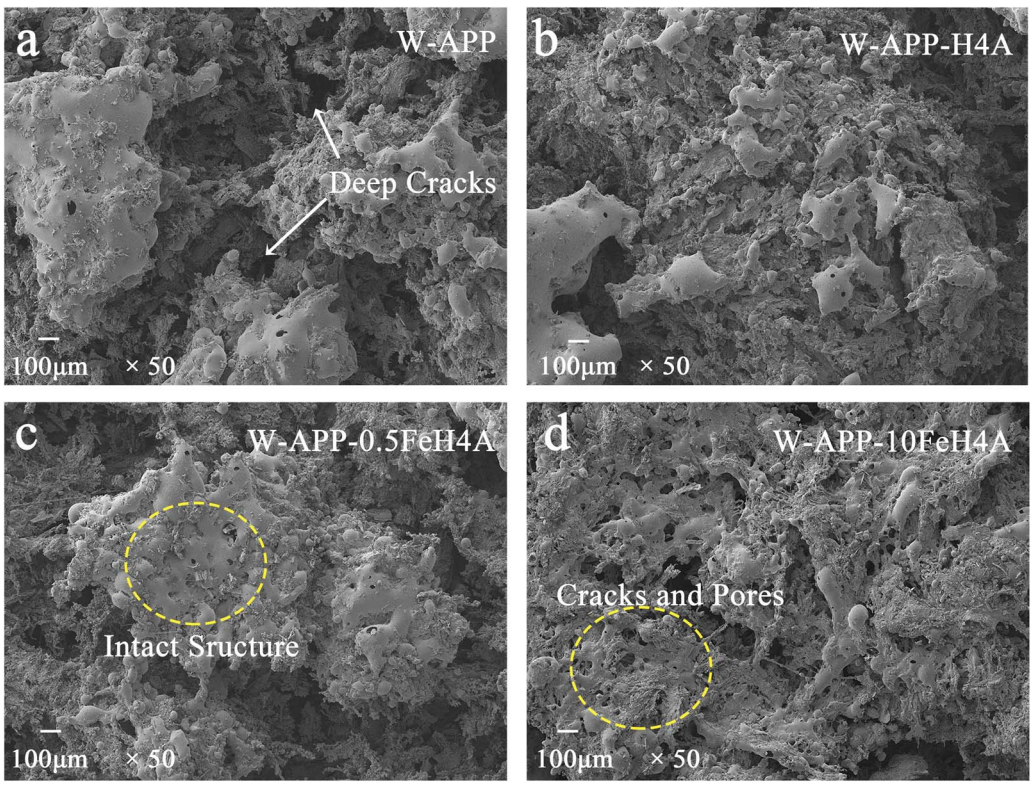

Fig. 9 Char residue of different samples after CCT ((a) W-APP; (b) W-APP-H4A; (c) W-APP-0.5FeH4A; (d) W-APP-10FeH4A).

(Fig. 9d). This could have a negative effect on the flame retardancy since the gaseous pyrolytic products can easily escape from the inner structure. These cracks on the surface char layer can be ascribed to the increased caused by the excessive iron oxide.[28] Therefore, with an appropriate amount of iron oxide, the modified H4A zeolites can facilitate the formation of an intact intumescent char layer, which improved flame retardancy effectively.

4. Conclusions

In this work, iron oxide-modified H4A zeolites were prepared using an impregnation method followed by calcination. Iron oxide was deposited on the surface and introduced into the inner part of the H4A zeolite during the modification process, resulting in a smaller mesopore diameter and a larger surface area. The degree of modification evidently affected the flame retardancy of wood composites. With proper modification, the first decomposition process of APP was accelerated and accordingly led to better flame retardancy of wood composites. However, when the modification degree was too high, the destroyed H4A zeolite framework and excess iron oxide in the residue affected the overall thermal stability of the char and exhibited a negative effect on flame retardancy. In addition, iron oxide-modified H4A zeolites improved smoke and CO suppression probably by catalyzing the conversion reaction of CO and other partially oxidized molecules owing to their larger surface area. Further studies proved that iron oxide-modified H4A zeolites play a role in both gaseous and condensed phase mechanisms during the combustion process. The results revealed the effect of iron oxide modification on the flame-retardant efficiency of H4A zeolites. We expect that this study will provide guidance for the design of high-performance flame retardants and synergists for wood composites.

Data availability

Data are available from the corresponding author upon reasonable request.

Author contributions

Shaodi Zhang: methodology; writing – original draft; formal analysis; investigation; analysis and interpretation of the data. Mingzhi Wang: conceptualization, supervision, writing – review & editing. Final approval of the version. Yuxiang Huang: investigation; writing – review & editing. Yahui Zhang: methodology; investigation. Wenji Yu: conceptualization; supervision; final approval of the version. All authors agree to be accountable for all aspects of the work.

Conflicts of interest

The authors declare that they have no known competing financial interests or personal relationships that could have appeared to influence the work reported in this paper.

Acknowledgements

This study was supported by the grants Chinese Academy of Forestry (CAFYBB2023QD001-03) and Key R&D Program of Shandong Province (grant number 2024TSGC0816).

References

1 T. Koddenberg, *Handbook of Wood Chemistry and Wood Composites*, 2016, vol. 110.
2 Y. Huang, K. Jiang, Y. He, J. Hu, K. Dyer, S. Chen, E. Akinlabi, D. Zhang, X. Zhang, Y. Yu, W. Yu and B. Bin Xu, *Adv. Mater.*, 2025, **2502266**, 1–11.
3 L. Lowden and T. Hull, *Fire Sci. Rev.*, 2013, **2**, 4.
4 C. M. Popescu and A. Pfriem, *Fire Mater.*, 2020, **44**, 100–111.
5 G. I. Mantanis, J. Martinka, C. Lykidis and L. Ševčík, *Wood Mater. Sci. Eng.*, 2020, **15**, 303–311.
6 J. Feng, L. Liu, Y. Zhang, Q. Wang, H. Liang, H. Wang and P. Song, *Exploration*, 2023, **3**, 20220088.
7 X. Peng, Y. Wu, W. Qu and H. Shi, *Chin. J. Wood Sci. Technol.*, 2025, **39**, 80–88.
8 M. Zhu, J. Zhu, J. Shi, M. Wen and Z. Zhao, *Chin. J. Wood Sci. Technol.*, 2021, **35**, 52–58.
9 P. Qin, D. Yi, J. Xing, M. Zhou and J. Hao, *J. Therm. Anal. Calorim.*, 2021, **146**, 2015–2025.
10 E. N. Kalali, L. Zhang, M. E. Shabestari, J. Croyal and D. Y. Wang, *Fire Saf. J.*, 2019, **107**, 210–216.
11 L. Zhang, S. Chen, Y. T. Pan, S. Zhang, S. Nie, P. Wei, X. Zhang, R. Wang and D. Y. Wang, *ACS Sustain. Chem. Eng.*, 2019, **7**, 9272–9280.
12 W. Wang, W. Zhang, H. Chen, S. Zhang and J. Li, *Constr. Build. Mater.*, 2015, **79**, 337–344.
13 S. Zhang, Z. Chen, M. Ding, T. Yang and M. Wang, *Constr. Build. Mater.*, 2020, **262**, 120754.
14 S. M. Auerbach, K. A. Carrado and P. K. Dutta, *Handbook of Zeolite Science and Technology*, 2003.
15 H. Demir, E. Arkiş, D. Balköse and S. Ülkü, *Polym. Degrad. Stab.*, 2005, **89**, 478–483.
16 S. Zhang, Y. Wu, X. Guo, H. Shen, M. Zhang and M. Wang, *BioResources*, 2019, **14**, 2013–2028.
17 S. Zhang, T. Yang, L. Li and M. Wang, *Micropor. Mesopor. Mater.*, 2021, **323**, 111191.
18 L. Wang, L. Song, Y. Hu and R. K. K. Yuen, *Ind. Eng. Chem. Res.*, 2013, **52**, 8062–8069.
19 W. Xu, B. Zhang, X. Wang, G. Wang and D. Ding, *J. Hazard. Mater.*, 2018, **343**, 364–375.
20 P. J. Davies, A. R. Horrocks and A. Alderson, *Polym. Degrad. Stab.*, 2005, **88**, 114–122.
21 X. Chen, L. Liu, J. Zhuo and C. Jiao, *J. Therm. Anal. Calorim.*, 2015, **119**, 625–633.
22 X. Chen, L. Liu and C. Jiao, *Adv. Polym. Technol.*, 2015, **34**, 1–9.
23 X. Chen, Y. Jiang and C. Jiao, *J. Hazard. Mater.*, 2014, **266**, 114–121.
24 Y. Sun, M. Gao, Z. Chai and H. Wang, *J. Therm. Anal. Calorim.*, 2018, **131**, 65–70.

25 G. Yang, J. Cai, Y. Geng, B. Xu and Q. Zhang, *ACS Sustain. Chem. Eng.*, 2020, **8**, 14365–14376.
26 L. Qian and Z. F. Yan, *Colloids Surf., A*, 2001, **180**, 311–316.
27 J. Wang, L. Liu, X. Dong, L. Alfilfil, C. E. Hsiung, Z. Liu and Y. Han, *Chem. Mater.*, 2018, **30**, 6361–6369.
28 Y. Zhang, X. Li, Z. Fang, T. R. Hull, A. Kelarakis and A. A. Stec, *Polym. Degrad. Stab.*, 2017, **136**, 139–145.
29 M. Choi, H. S. Cho, R. Srivastava, C. Venkatesan, D. H. Choi and R. Ryoo, *Nat. Mater.*, 2006, **5**, 718–723.
30 K. Cho, H. S. Cho, L. C. De Ménorval and R. Ryoo, *Chem. Mater.*, 2009, **21**, 5664–5673.
31 D. P. Serrano, J. M. Escola and P. Pizarro, *Chem. Soc. Rev.*, 2013, **42**, 4004–4035.
32 J. Gong, K. Yao, J. Liu, Z. Jiang, X. Chen, X. Wen, E. Mijowska, N. Tian and T. Tang, *J. Mater. Chem. A*, 2013, **1**, 5247–5255.
33 H. Zeng, L. Zhai, J. Zhang and D. Li, *Sci. Total Environ.*, 2021, **753**, 142002.
34 A. Mockovčiaková, Z. Orolínová, M. Matik, P. Hudec and E. Kmecová, *Acta Montan. Slovaca*, 2006, **1**, 353–357.
35 B.-r. Zhuang, Y.-p. Zhan, W.-y. Huang, H.-l. Ye and Y.-q. Xie, *J. Hazard. Mater.*, 2018, **357**, 271–278.
36 S. Royer and D. Duprez, *ChemCatChem*, 2011, **3**, 24–65.
37 G. Camino, L. Costa and L. Trossarelli, *Polym. Degrad. Stab.*, 1985, **12**, 203–211.
38 P. Wei, P. Jiang, Z. Han and J. Wang, *J. Fire Sci.*, 2005, **23**, 173–184.
39 H. Yang, R. Yan, H. Chen, D. H. Lee and C. Zheng, *Fuel*, 2007, **86**, 1781–1788.
40 X. Ye, J. Li, W. Zhang, R. Yang and J. Li, *Composites, Part B*, 2020, **191**, 107961.
41 T. Ma, L. Li, Q. Wang and C. Guo, *Composites, Part B*, 2020, **183**, 107697.
42 F. X. Collard, A. Bensakhria, M. Drobek, G. Volle and J. Blin, *Biomass Bioenergy*, 2015, **80**, 52–62.